Edge poloidal rotation profiles of H-mode plasmas in the JFT-2M tokamak

Cite as: Physics of Fluids B: Plasma Physics **4**, 2552 (1992); https://doi.org/10.1063/1.860486
Submitted: 12 November 1991 • Accepted: 11 March 1992 • Published Online: 04 June 1998

K. Ida, S. Hidekuma, M. Kojima, et al.

Edge poloidal rotation profiles of H-mode plasmas in the JFT-2M tokamak

K. Ida, S. Hidekuma, and M. Kojima
National Institute for Fusion Science, Nagoya, 464-01, Japan

Y. Miura, S. Tsuji, K. Hoshino, M. Mori, N. Suzuki, T. Yamauchi, and the JFT-2M Group
Japan Atomic Energy Research Institute, Naka-machi, Naka-gun, Ibaraki, 319-11, Japan

(Received 12 November 1991; accepted 11 March 1992)

Parameter dependence of the radial structure of edge poloidal rotation is studied with spectroscopic measurements for L- and H-mode plasmas in the JFT-2M tokamak [Y. Miura *et al.*, in *Plasma Physics and Controlled Nuclear Fusion Research*, Proceedings of the 13th International Conference, Washington 1990 (IAEA, Vienna, 1991), Vol. 1, p. 325]. The poloidal flow is in the electron diamagnetic direction and appears suddenly near the plasma edge at the H-mode transition. The poloidal rotation velocity profile in the H mode has a peak at the separatrix. No critical normalized ion collisionality, ν_{*i}, for the transition of the L to the H mode is observed. The size of the poloidal flow in the H mode has no dependence on the poloidal gyroradius.

I. INTRODUCTION

Since the sudden transition from low confinement (L mode) to high confinement (H mode) was discovered in ASDEX,[1] it has been observed in many tokamaks,[2–7] with several heating and operational schemes.[8–11] The H-mode transition is characterized by an improvement in both particle and energy confinement. A rapid increase in density in conjunction with a sudden drop of the H_α/D_α recycling light is a common H-mode characteristic. Recently the poloidal rotation velocity and the radial electric field near the plasma periphery have been found to play an important role in the L- to H-mode transition.[12–17] The L/H transition can be triggered by driving a radial current across the outer magnetic surface.[12] The driving current and radial electric field imposed by electrodes can be positive or negative in the H mode.[13] However, without an external driving current, the sudden change of edge poloidal rotation velocity is in the electron diamagnetic direction, which indicates a sudden increase of the negative radial electric field, as was observed at the L- to H-mode transitions in DIII-D.[14] The L- to H-mode transition is also associated with a sudden decrease in the edge density and magnetic fluctuation levels.[15,16] This negative radial electric field may be driven by the large outward fluxes of ions, such as thermal and/or fast ion loss at the plasma edge, since the poloidal rotation velocity measured in the H mode is much larger than neoclassical predictions. More recently, profiles of the radial electric field at the plasma edge were measured in JFT-2M and preliminary results were reported.[17]

Various theoretical models for the L- to H-mode transition have been proposed since the discovery of the H mode. Recently, models based on bipolar ion orbit loss,[18–20] neoclassical viscosity,[21,22] spontaneous poloidal spin-up,[23] or power flow asymmetry[24] fluctuation suppression[25] have been proposed to explain the sudden change of poloidal rotation velocity at the L/H transition. However, predicted features of poloidal rotation velocity and the radial electric field are different among the various models. It is, therefore, crucial to study precise profiles of poloidal flow and parameter dependence of poloidal rotation and the radial electric field at L/H transitions. In this paper we present more details of previous results,[17] and discuss comparisons with several current theories.

II. MEASUREMENTS OF POLOIDAL FLOW AND RADIAL ELECTRIC FIELD

The radial electric field profiles are inferred from poloidal and toroidal rotation and ion pressure profiles using the ion momentum balance equation;

$$E_r=\frac{\partial p_i}{eZ_i n_i \partial r}-(B_\theta V_\varphi - B_\varphi V_\theta), \tag{1}$$

where Z_i, p_i, n_i are the ion charge, pressure, and density, B_φ and B_θ the toroidal and poloidal magnetic fields, and v_φ and v_θ the toroidal and poloidal rotation velocities. Toroidal rotation velocity is of the same order as poloidal rotation velocity at the plasma edge. The contribution of toroidal rotation velocity to the electric field is much smaller than that of poloidal rotation velocity, since the poloidal magnetic field is smaller than the toroidal magnetic field by one order of magnitude. The dominant impurity in JFT-2M is carbon and its amount is estimated from the intensity of emission from hydrogenlike carbon, C^{5+}, (CVI). The radial electric field is estimated using the momentum balance equation for carbon, since there is no guarantee that bulk ions rotate with the same velocity as carbon when the plasma changes quickly at the L/H transition.[26]

The toroidal rotation velocity, ion temperature, and fully stripped carbon density profiles are measured using the charge exchange spectroscopy technique at CVI 5292 Å with two toroidal arrays (each of 34 channels) having a spatial resolution of 1 cm. The poloidal rotation and edge ion temperature profiles are measured using the intrinsic radiation of CVI at 5292 Å. The two sets of toroidal/poloidal arrays view the plasma in opposite directions to define the zero reference for Doppler shift measurements. The poloidal arrays (two set of 23 channels) do not view

 0899-8213/92/082552-08$04.00

across the beamline and view only the plasma periphery with a spatial resolution of 4 mm. The integration effect of the line of sight in the poloidal arrays is small, as long as the signal increases rapidly with decreasing minor radius, even though the emission shell extends well inside the plasma. However, in order to avoid this problem completely, a wavelength-resolved Abel inversion[27] is used to obtain local ion temperature and poloidal rotation velocity from the poloidal arrays.

The optical fibers (114 channels) are led to the entrance slit of a 1 m Czerny–Turner spectrometer with a 2160 mm grating. The 114 fibers are arranged along the height of the entrance slit. The diameter of each fiber is 0.125 mm. The fibers are arranged with two rows side by side to give the slit width of 0.25 mm for poloidal and edge toroidal channels. For the central toroidal channels that are viewing the high ion temperature region of the plasma, four rows of fibers are used to give a slit width of 0.5 mm. A charge coupled device (CCD) detector with a time resolution of 16.7 msec is coupled to an image intensifier (microchannel plate) by an image fiber bundle and is arranged at the exit plane of the spectrometer. An extensive spatial calibration of the 114 channels has been done using a mercury pen lamp outside the vacuum vessel through window. In order to obtain an accurate correspondence between points in the spectrometer output image and individual fibers at the input, we take a fiber for each end of the input bundle and illuminate it with a mercury lamp. The two spots obtained at the output of the spectrometer precisely determine the position of the ends of the input array. The location of the spot from the mercury lamp on the CCD detector was measured and this data used for the position calibration. The absolute uncertainty in position is less than 5 mm, while the relative accuracy is confirmed by the fact that the position of the sharp increase of CVI emission from the toroidal arrays agrees with that measured in the poloidal arrays. The uncertainty of the position of the separatrix calculated with an equilibrium code is also estimated to be 5 mm. The fine-structure components due to different one-level states increases the apparent Doppler width in the measurements of low ion temperatures. This results in an increase of apparent ion temperature from real temperature of 15% at 100 eV for the $\Delta n=8$–7 transition.[28] The correction due to fine structure is taken into account in our analysis, however, it is of minor significance compared with the uncertainty in the fitting of the measured spectrum.

The profile of electron temperature and its gradient are measured with an electron cyclotron emission (ECE) radiometer to establish the location of the thermal transport barrier. The plasma near the periphery ($r/a>0.9$) is not optically thick for emission at the second harmonic of the electron cyclotron frequency. The ECE temperature at this location is not accurate unless the emission is reflected at the wall, making the plasma effectively more optically thick. The reflection coefficient determined from the intensity ratio of the second to third harmonic ECE signal is 0.88 in JFT-2M.[29] The electron temperature at the plasma edge is found to be underestimated by 20%–30%. The

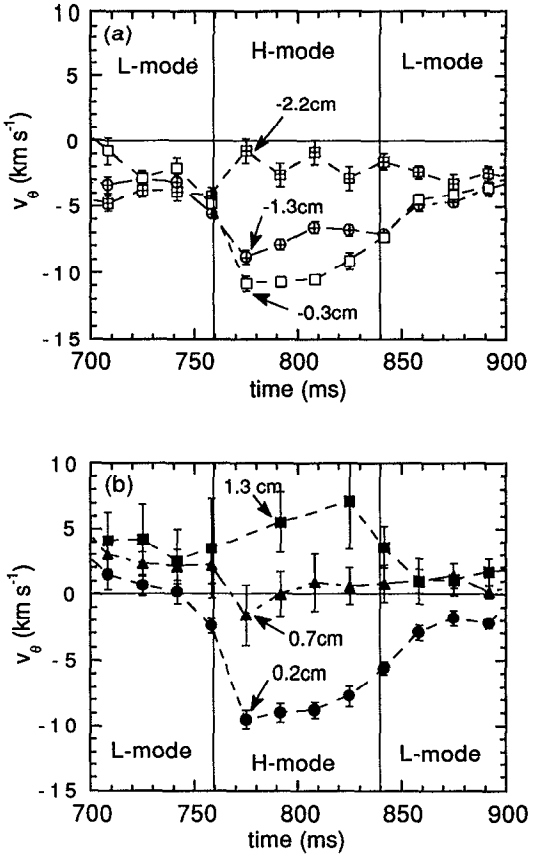

FIG. 1. Time evolution of poloidal rotation velocity at (a) -0.3, -1.3, and -2.2 cm inside and (b) 0.2, 0.7, and 1.3 cm outside the separatrix. The L to H and H to L transitions occur at $t=760$ and 840 msec.

spatial resolution of the measurements, set by the frequency bandwidth of the detector, is 3 mm. Bulk electron density (n_e) and temperature (T_e) are measured with Thomson scattering. The edge plasma space potential profiles are derived from T_e and floating potential measurements from a Langmuir probe outside the separatrix.

III. RADIAL STRUCTURE OF POLOIDAL FLOW AND RADIAL ELECTRIC FIELD

Figure 1 shows the time evolution of the poloidal rotation velocity for a hydrogen plasma with a current of 280 kA, a toroidal field of 1.3 T, q_ψ of 2.7, a major radius of 1.3 m, and a minor radius of 0.3 m in a single null divertor configuration. Neutral beam injection (NBI) starts at 700 msec in the codirection with a power of 0.7 MW, and a second beam is added at 730 msec in the counterdirection with a power of 0.3 MW to exceed the power threshold for L/H transition that occurs at 760 msec. A large jump of poloidal rotation velocity at the L/H transition is observed near the separatrix, [in the -0.3 cm (inside) and $+0.2$ cm (outside) channels], while the changes of poloidal rotation velocity become small away from the separatrix, as seen in the -2.2 and $+0.7$ cm channels. The poloidal rotation increases in the electron diamagnetic direction in the H mode, regardless of the direction of plasma current and neutral beam injection. The change of poloidal rotation is

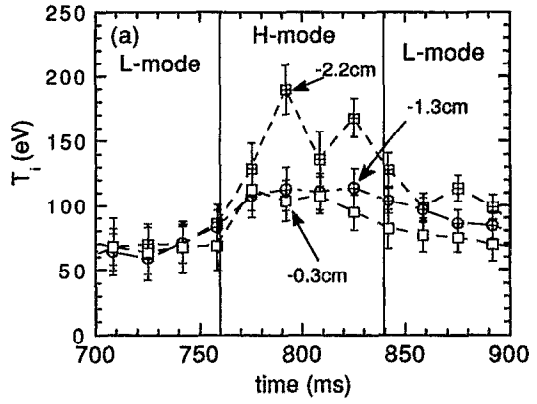

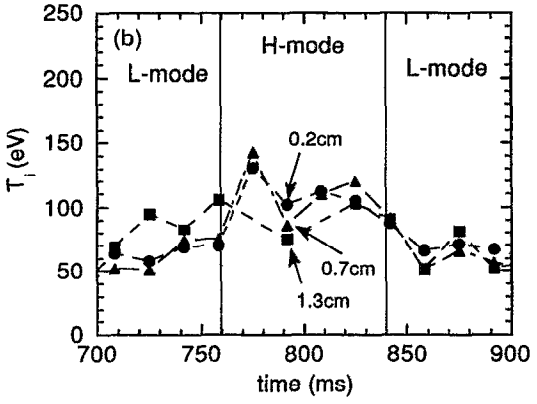

FIG. 2. Time evolution of the ion temperature at (a) -0.3, -1.3, and -2.2 cm inside and (b) 0.2, 0.7, and 1.3 cm outside the separatrix. The L to H and H to L transition occur at $t=760$ and 840 msec.

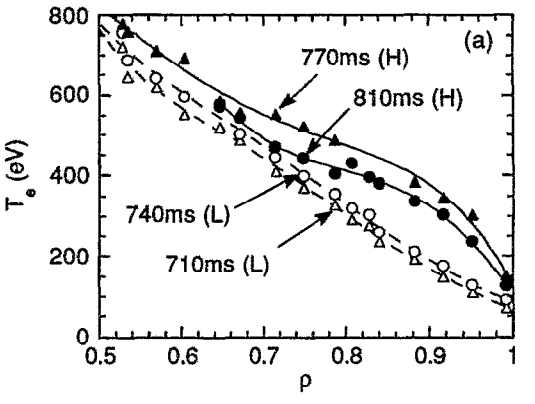

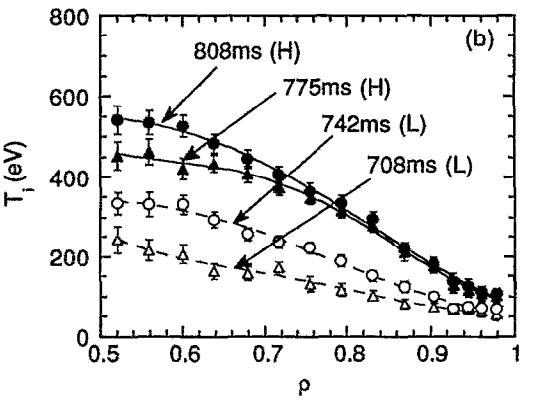

FIG. 3. Radial profiles of (a) electron temperature measured with the ECE radiometer and (b) ion temperature measured with toroidal arrays at $t=708$ and 742 msec (before the L/H transition) and $t=775$ and 808 msec (after the L/H transition). Here ρ is an averaged minor radius.

fairly localized near the separatrix, while the sharp gradient in the ion temperature is observed further inside the separatrix, as shown in Fig. 2. The ion temperature at $ds=-2.2$ cm increases significantly 50 msec after the L/H transition.

The profiles of ion and electron temperature before ($t=708$ and 742 msec) and after ($t=775$ and 808 msec) the L/H transition are shown in Fig. 3. Both electron and ion temperature profiles show a larger pedestal at a normalized minor radius of 0.9 during the H-mode phase. The increase of electron temperature is simply due to the improvement of electron thermal transport, since most NBI power is deposited near the plasma center both in L-mode and H-mode phase. However, the increase of central ion temperature in the H-mode phase is due to both the improvement of ion energy transport and the increase of power flow from electrons at higher electron density. The electric field profiles for Ohmic, L-mode, and H-mode plasmas are calculated from rotation velocities and pressure gradients of carbon using the momentum balance equation for C^{5+} [Eq. (1)]. The electric field becomes more negative in the H mode, due to an increase of poloidal rotation in the electron diamagnetic direction. The poloidal rotation velocity profiles and ion temperature profiles at Ohmic ($t=692$ msec), L mode ($t=742$ msec), and H mode ($t=792$ msec) are shown in Fig. 4. The plasma always rotates in the ion diamagnetic direction outside the separatrix and in the electron diamagnetic direction inside the separatrix. The structure of poloidal flow is consistent with the measurements of phase velocity of the turbulent fluctuations in Texas Experimental tokamak (TEXT).[30] The position, where the plasma does not rotate poloidally, moves outward as the plasma changes from Ohmic to the L to the H mode. The poloidal flows outside and inside the separatrix are in the opposite direction to each other.

The gradient of the electric field inside the separatrix, $ds=-1.5$ cm, is positive in the Ohmic phase, slightly positive in the L mode, and becomes negative in the H mode. The relative space potentials in the plasma are derived by integrating the radial electric field. Combining the measurements of space potential with electric probes, the profiles of space potential for Ohmic, L mode and H mode are obtained, as shown in Fig. 5(b). The space potentials just inside the separatrix are positive in Ohmic and the L mode and negative in the H mode. This negative space potential is -260 V, while the ion temperature is 170 eV at the thermal barrier. These measurements indicate that the improvement of thermal transport correlates with the negative $\partial E_r/\partial r$. In conclusion, both E_r and $\partial E_r/\partial r$ become more negative in the thermal barrier, 1–2 cm inside the

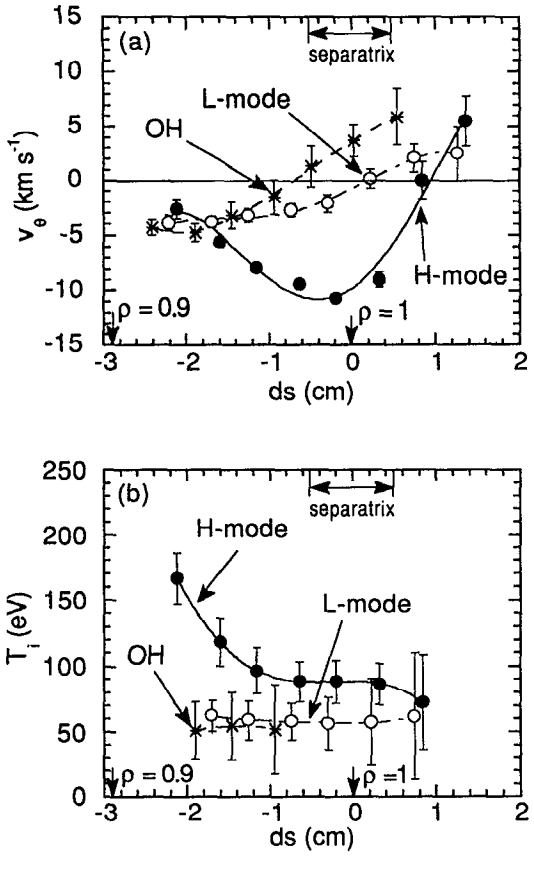

FIG. 4. Radial profile of (a) edge poloidal rotation velocity and (b) ion temperature as a function of the distance from the separatrix (ds), for OH (t=692 msec, asterisk), for the L mode (t=742 msec, open circles), and for the H mode (t=792 msec, closed symbols). Negative value of ds stands for the distance inside and positive value stands for the distance outside the separatrix.

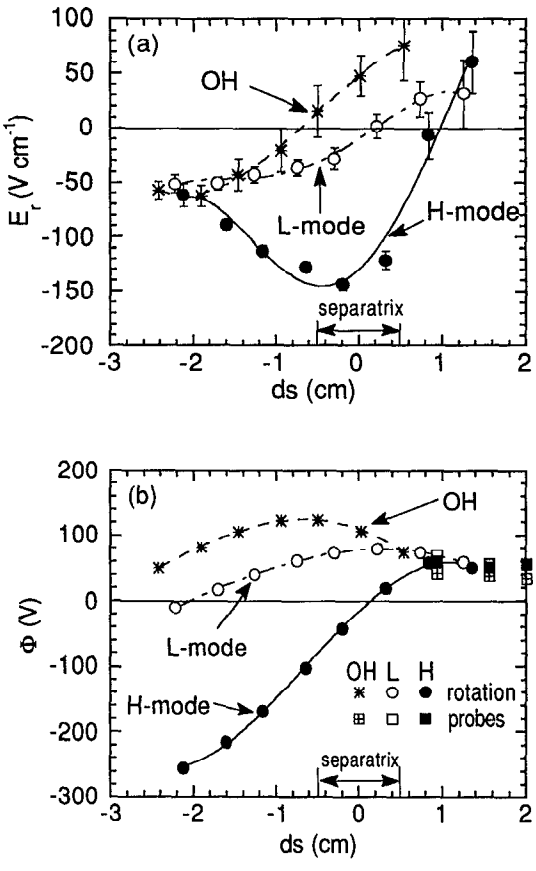

FIG. 5. Radial profile of (a) edge radial electric field and (b) space potential as a function of the distance from the separatrix (ds), for OH (t=692 msec, asterisk) the L mode (t=742 msec, open symbols), and the H mode (t=792 msec, closed symbols). The absolute value of the space potential is measured by probes (squares symbols).

separatrix, after the L/H transition. Positive $\partial E_r/\partial r$ is observed outside the separatrix both for L- and H-mode plasmas.

IV. VELOCITY SHEAR AND THE THERMAL BARRIER

The ion thermal transport barrier is always found at 1–2 cm inside the separatrix, although the steep gradients of electron density and the brightness of CVI emission occur near the plasma edge, within 0.5 cm of the separatrix. Figure 6 shows the gradient of electron and ion temperature as a function of poloidal rotation velocity shear 1.5 cm inside the separatrix for various discharges. Poloidal rotation shear is positive or a little negative $\partial v_\theta/\partial r > -2$ km sec^{-1} cm^{-1}, with small gradients of electron and ion temperature, $|\partial T_e/\partial r| < 40$ eV/cm and $|\partial T_i/\partial r| < 20$ eV/cm, for L-mode plasmas. On the other hand, the poloidal rotation shear is always negative during large gradients of electron and ion temperature, 40 eV/cm $< |\partial T_e/\partial r| < 90$ eV/cm, 20 eV/cm $< |\partial T_i/\partial r| < 70$ eV/cm, in the H-mode plasma. Both the electron temperature gradient and poloidal rotation velocity shear become larger as the plasma current of the discharge is increased from 170 to 280 kA.

The large electron temperature gradient is associated with negative poloidal rotation velocity shear not positive rotation shear. This sign dependence of poloidal rotation shear on the improvement of heat transport is one of the important characteristics in the L/H transition of the plasma with no externally driven electric field. The ion temperature gradients show similar behavior, but the gradients of ion temperature are slightly smaller than the electron temperature gradient. This is consistent, in that most of the heating power of the neutral beam is into the electrons, so at the plasma edge low-temperature ions are heated through collision with electrons.

Bulk ion temperatures and rotation velocities are assumed to be the same as the carbon temperatures and rotation velocities. In order to obtain a wide range of ion normalized collisionality, poloidal rotation velocities were measured for H-mode discharges with various electron densities and plasma currents. The poloidal rotation parameter U_p($= v_\theta B/v_{th}B_\theta$) is plotted as a function of normalized ion collisionality in Fig. 7. The ion collisionality ν_{*i} at 0.7 cm inside the separatrix is obtained with the edge ion temperature measured with CVI line and the edge electron density extrapolated from far infrared (FIR) interferometer measurements. The extrapolated edge densities are

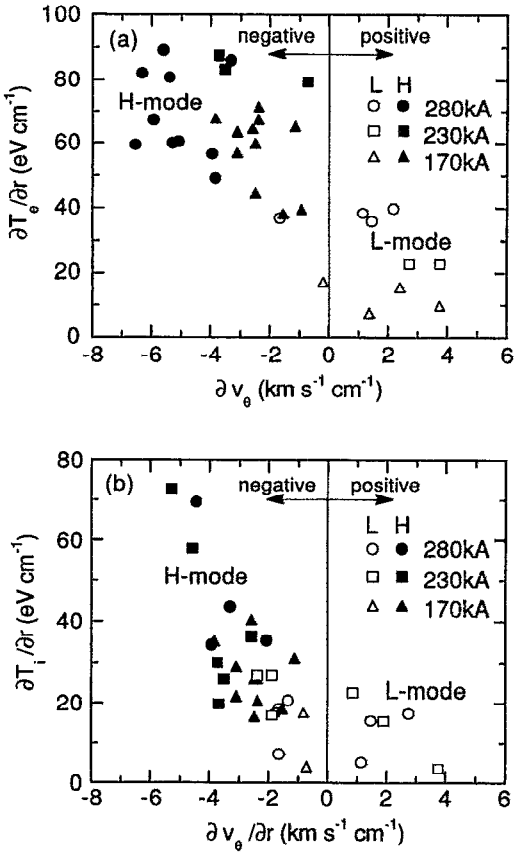

FIG. 6. Gradients of (a) electron temperature measured with the ECE radiometer and (b) ion temperature 1.5 cm inside the separatrix as a function of poloidal rotation velocity shear. Open symbols stand for the L mode and closed symbols for the H mode. Circles are discharges with the plasma current of 280 kA and triangles are with 170 kA. Squares stand for limiter discharges with plasma current of 230 kA.

consistent with the probe measurements. The ion collisionality ν_{*i} decreases after the L/H transition for the discharges with higher plasma current, while it increases or does not change for lower plasma current. This is mainly due to the fact that the ion temperature increases more than the electron density for higher current, but increases less than the electron density for lower current. The poloidal rotation parameter changes from below 2 to above 2 at L to H transitions. Although there is no critical ion collisionality for the L/H transition, critical values of the poloidal rotation parameter are observed. This critical poloidal rotation parameter, U_p, at the L/H transition is 2–3. We note that the range of edge ion temperature and B/B_θ in JFT-2M are too narrow, at most a factor of 2, to distinguish whether the critical parameter is poloidal rotation velocity or U_p.

Figure 8 shows the width of the poloidal rotation shear for various poloidal gyroradius width $\rho_{\theta i}$ with plasma current of 170 to 280 kA and with hydrogen and deuterium working gas. The widths of poloidal rotation velocity, $L(v_\theta)$, is defined as twice of the full width at half-maximum (FWHM) of the poloidal rotation velocity profile in the H mode. It is ~4 cm over a wide range of

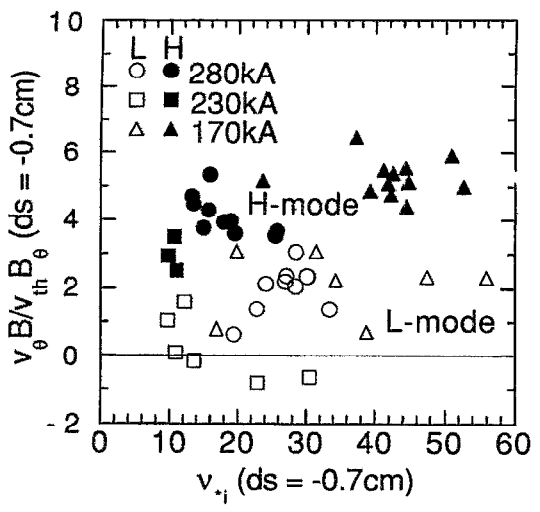

FIG. 7. Normalized poloidal rotation velocity as a function of normalized ion collisionality. Open symbols stand for the L mode and closed symbols for the H mode. Circles are discharges with a plasma current of 280 kA and triangles are with 170 kA. Squares stand for a limiter discharges with a plasma current of 230 kA.

poloidal gyroradius from 0.7 to 2 cm. The width of the poloidal rotation velocity shear profile is two to six poloidal gyroradii, however, it shows no dependence on gyroradius.

V. DISCUSSIONS

Since several H-mode models have been proposed, we now discuss the agreements and discrepancies between each model and our observations. Comparisons of characteristic parameters in the H-mode plasma between JFT-2M measurements and the various theories are summarized in Table I. The L/H transition in question is purely the spon-

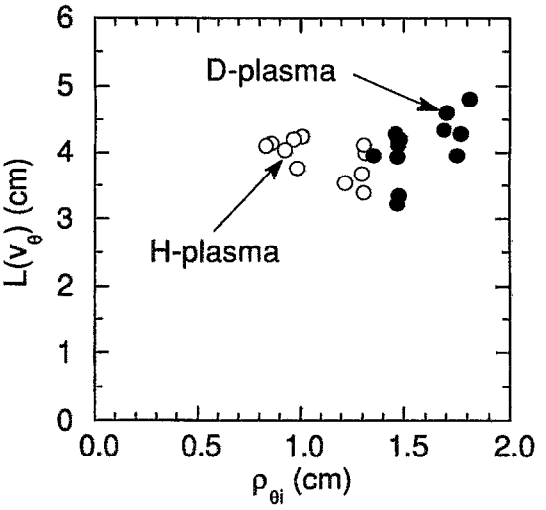

FIG. 8. The width of the poloidal rotation velocity shear, $L(v_\theta)$, as a function of poloidal gyroradius Open circles are for the hydrogen plasma and closed circles are for the deuterium plasma.

TABLE I. Comparison of characteristic parameters in the H-mode plasma between measurements and theories.

Parameters	Experiment	Itoh	Shaing	Biglari	Hassam	Tendler
E_r	Negative (no induced current)	Positive (negative, if $\partial E_r/\partial r < 0$)	Negative	Not important		Negative
$\partial E_r/\partial r$	Negative	Negative	Positive	Positive or negative		
E_r in SOL	Positive					Positive
Critical pressure gradient λ	~ 1	~ 1			Critical density gradient	
Critical ν_{*i}	None	None	$1\sim 2$ if no fast ion loss	None	None	
Critical $\lvert\partial v_\theta/\partial r\rvert$	None	None	None	Necessity	None	
Electric field	$>-0.5\sim 0$ (L)	1.0 (L)				
Shear u_g	$<-0.5\sim 0$ (H)	-2.3 (H)				
Poloidal velocity U_p	$<2\sim 3$ (L)		1 (L)			
	$>2\sim 3$ (H)		3 (H)			
Dependence of shear region on poloidal gyroradius	No	Yes	Yes (no, if orbit is squeezed)	No	No	

taneous transition during plasma heating. These transitions must have features different from the L/H transitions triggered by driving a radial current across the outer magnetic surface.[12,13] The radial electric field inside the separatrix is negative in the spontaneous H mode, as observed in JFT-2M, although it can be negative or positive when the driving current is induced and a radial electric field is imposed externally.[13]

In Itoh's model, loss of electrons driven by turbulence is balanced against the orbit loss of trapped ions.[18–20] This particle balance equation determines the self-consistent radial electric field. The microturbulence is stabilized for negative electric field shear $\partial E_r/\partial r<0$, and the electron anomalous flux is reduced by the factor of $(1 + u_g/u_c)^{1/2}$, where u_g is the shear parameter of the electric field and is defined as $\rho_{\theta i}(\partial E_r/\partial r)/(v_{\rm th}B_\theta)$, and the critical parameter u_c is 2.7 in JFT-2M. On the other hand, the banana width of trapped ions is also reduced with negative electric field shear by the factor of $(|1-u_g|+C\epsilon)^{-1/2}$, where ϵ is the inverse aspect ratio and C is a numerical coefficient, which determines the minimum size of the banana width. The model predicts positive E_r shear, $u_g 0,r$ for large ion and electron fluxes in the L mode, and negative E_r shear, $u_g 0,r$ for reduced particle fluxes in the H mode. The predicted shear parameter u_g is 1.0 in the L mode and -2.3 in the H mode.[20] In this model the transition from the L to H mode is predicted to take place when the scale length of the edge pressure profile becomes smaller than the poloidal ion gyroradius, i.e., $\lambda>1$, where λ is a pressure gradient parameter defined as

$$-\left(\frac{T_e}{T_i}\right)\rho_{\theta i}\left[\left(\frac{(\partial n_e/\partial r)}{n_e}+\frac{\alpha(\partial T_e/\partial r)}{T_e}\right)\right],$$

and α is a numerical constant of the order of unity.

The measured shear parameter u_g is in the range of $-0.5 < u_g < 1$ for the L mode and $-2 < u_g < -0.5$ for the H mode at 0.7 cm inside the separatrix. These values of the shear parameter u_g are consistent with the prediction. The pressure gradient parameter λ changes from below unity (~ 0.5) to above unity (~ 1.3) at the L/H transition and is consistent with the critical value of their model ($\lambda_c \approx 1$). We observe qualitative agreement of characteristic parameters u_g and λ_c in Itoh's model at the L/H transition. However, the lack of dependence of the width of the sheared flow region on the poloidal gyroradius contradicts their model.

Shaing shows that the poloidal momentum balance equation has bifurcated solutions.[21] The poloidal torque due to the loss of trapped ions is balanced by the neoclassical parallel (poloidal) viscosity. Since the neoclassical parallel (poloidal) viscosity has a peak around $U_p \sim 1$, once the poloidal rotation velocity exceeds this critical value, the plasma can rotate in the electron diamagnetic direction with a larger speed at a fixed poloidal torque. By taking account of the change of the poloidal torque due to the change of speed, his model predicts $U_p \sim 1$ for the L mode (before the L/H transition) and 2 for the H mode (after the transition). The corresponding large negative, not positive, radial electric field E_r is expected to suppress the fluctuations.[22] In the model, collisionality required to achieve consistent ion orbit loss rate at the L/H transition varies with machine geometry, and is predicted to be $\nu_{*i} = 1$–2 in JFT-2M.

The critical poloidal rotation speed measured in JFT-2M agree with the prediction of Shaing's model within a factor of 2. However, the normalized ion collisionality, ν_{*i}, measured in the JFT-2M tokamak is 10–60 at the L/H transition, and does not agree with the prediction of his model. This discrepancy implies that fast ion losses, which are not included in his model, may trigger the L- to H-mode transition. When the fast ion loss, which is independent of ν_{*i}, becomes dominant, the L- to H-mode transi-

tion can take place at any ν_{*i} values.[31] We observe a qualitative agreement of the characteristic parameter U_p in Shaing's model[21] at the L/H transition. However, the model that includes fast ion loss as well as bulk ions is necessary to achieve better agreement with the experimental observations. The sign dependence of transport improvement on poloidal rotation velocity shear observed in JFT-2M is consistent with Shaing's model, because it predicts the suppression of fluctuations with a more negative electric field, not with positive E_r.[22] As shown in Fig. 8, the width of poloidal rotation shear does not depend on a poloidal gyroradius. This fact seems to be inconsistent with the ion orbit loss model.[18–22] Recently, the complete effects of orbit squeezing has been studied, and it has been found theoretically that the width of the edge radial electric field layer in the H mode, as estimated from the ion orbit loss model, does not depend explicitly on the poloidal gyroradius.[32]

Hassam proposes an H-mode model based on a poloidal spin-up of the plasma caused by poloidally asymmetric particle flux.[23] In his model, when the poloidal asymmetry—the fractional difference between the particle transport inside and outside—is sufficiently large, and the particle transport rate is larger than the damping due to magnetic pumping, spontaneous poloidal spin-up occurs. This spin-up is characterized by simultaneous sudden changes in both poloidal and toroidal flow velocity. His model does not rely on a nonambipolar flux such as edge ion loss, and has two important features: (1) the width of the spin-up layer does not depend explicitly on the poloidal gyroradius; and (2) the L/H transition does not depend on the ion collisionality parameter, that is, the poloidal spin-up may occur over a wide range of ν_{*i}. The experimental data shown in Figs. 7 and 8 are quite consistent with these features of his model. However, no simultaneous change of both poloidal and toroidal rotation velocity has been observed, at least in the JFT-2M H mode.

None of these models can fully explain the structure of the edge electric field, negative $\partial E_r/\partial r$ inside and positive $\partial E_r/\partial r$ outside the separatrix, since they solve problems only inside the separatrix. Tendler deals with the problem both inside and outside the separatrix, in the scrape-off layer (SOL) with the divertor configuration.[24] Owing to the inhomogeneity of the diffusion, significant variation of the plasma density and potential exists along field lines near the separatrix. The plasma is moved radially by the variation of potential (poloidal electric field directed toward the X point). On the other hand, the radial electric field arising from the radial inhomogeneity of the plasma temperature causes a poloidal rotation. The flow pattern is determined by these radial and poloidal electric fields. According to his model, the poloidal flow becomes convective; i.e., the poloidal flow on the inner flux surface just inside the separatrix is in the electron diamagnetic direction, as predicted by neoclassical theory. The flow crosses the separatrix near the X point and returns along the SOL in the ion diamagnetic direction. The sign reversal of poloidal flow between the inside and outside of the separatrix, as seen in Fig. 4, is not inconsistent with the Tendler model. However, his model fails to explain the H mode in the limiter configuration, where no X point exists. Experimentally, the poloidal flow in the limiter H mode is similar to that in the divertor H mode. In order to compare the measurements with this model in more detail, measurements of the two-dimensional (2-D) poloidal flow pattern in the vicinity of the separatrix would be necessary.

The influence of sheared poloidal rotation in H-mode plasmas has been investigated by Biglari, and turbulence is expected to be suppressed by poloidal velocity (radial electric field) shear.[25] His theory predicts that both negative ($\partial E_r/\partial r < 0$) and positive ($\partial E_r/\partial r > 0$) electric field shear can suppress the fluctuations, if $|\partial v_\theta/\partial r|$ becomes large enough; $|\partial v_\theta/\partial r| > |\omega/(k_\theta L_r)|$, where ω is a decorrelation frequency, k_θ is a poloidal wave number, and L_r is a radial correlation length of fluctuations. However, clear sign dependence of improvement of thermal transport on $\partial E_r/\partial r$ and $\partial v_\theta/\partial r$ is observed. The L- to H-mode transition is observed only when the velocity shear becomes negative, not when the velocity shear is positive. There is no critical $|\partial v_\theta/\partial r|$ for L/H transition. The second derivative of E_r becomes significant in the H mode, $\partial E_r^2/\partial r^2 > 0$, although it is much smaller in the L mode. This fact implies that $\partial E_r^2/\partial r^2$ is more important than $\partial E_r/\partial r$ in stabilizing fluctuations, if the improvement of thermal transport is purely due to the suppression of fluctuations.

In conclusion, two opposite poloidal flows are observed in the vicinity of the separatrix. Flow is in the electron diamagnetic direction inside and ion diamagnetic direction outside the separatrix. The poloidal flow inside increases in magnitude and has a peak close to the separatrix in the H mode. The thermal barrier, which is indicated by a large gradient of both electron and ion temperature, is only associated with a negative electric field shear ($\partial E_r/\partial r < 0$). The L- to H-mode transition can occur over wide range of ion collisionality ($\nu_{*i} = 10$–60) in the JFT-2M plasma. No dependence of the width of the sheared poloidal flow on the poloidal gyroradius is observed, which suggests that H-mode theories related to ion orbit loss should be modified.

ACKNOWLEDGMENTS

The authors would like to thank Dr. S.-I. Itoh, Dr. K. Itoh [National Institute for Fusion Science (NIFS)], K. C. Shaing (Oak Ridge National Laboratory), and A. Leonard (General Atomics) for their useful discussions. The authors also thank T. Matsuda [Japan Atomic Energy Research Institute (JAERI)] for data acquisition, Dr. T. Yamauchi, Dr. H. Tamai, Dr. H. Ogawa (JAERI) for the operation of the diagnostic and the tokamak and NBI operation staff at JFT-2M. Continuous encouragement by Dr. H. Maeda (JAERI), Dr. Y. Hamada (NIFS), and Dr. K. Matsuoka (NIFS) is acknowledged. The authors thank Dr. N. Hawkes (Culham Laboratory) for correcting the manuscript.

[1] F. Wagner, G. Becker, K. Behringer, D. Campbell, A. Eberhangen, W. Engelhardt, G. Fussmann, O. Gehre, J. Gernhardt, G. v. Gierke, G. Haas, M. Huang, F. Karger, M. Keilhacker, O. Kluber, M. Kornherr,

K. Lackner, G. Lisitano, G. G. Lister, H. M. Mayer, D. Meisel, E. R. Muller, H. Murmann, H. Niedermeyer, W. Poschenrieder, H. Rapp, H. Rohr, F. Schneider, G. Siller, E. Speth, A. Stabler, K. H. Steuer, G. Venus, and O. Vollmer, Phys. Rev. Lett. **49**, 1408 (1982).

[2]S. M. Kaye, M. G. Bell, K. Bol, D. Boyd, K. Brau, D. Buchenauer, R. Budny, A. Cavallo, P. Couture, T. Crowley, D. S. Darrow, H. Eubank, R. J. Fonck, R. Goldston, B. Grek, K. P. Jaehnig, D. Johnson, R. Kaita, H. Kugel, B. LeBlanc, J. Manicam, D. Manos, D. Mansfield, E. Mazzucato, R. McCann, D. McCune, K. McGuire, D. Mueller, A. Murdock, M. Okabayashi, K. Okano, D. K. Owens, D. E. Post, M. Reusch, G. L. Schmidt, S. Sesnic, R. Slusher, S. Suckewer, C. Surko, H. Takahashi, F. Tenney, H. Towner, and J. Valley, J. Nucl. Mater. **121**, 115 (1984).

[3]M. Nagami, M. Kasai, A. Kitsunezaki, T. Kobayashi, S. Konoshima, T. Matsuda, M. Miya, H. Ninomiya, S. Sengoku, M. Shimada, H. Yokomizo, T. Anmgel, C. Armentrout, F. Blau, G. Bramson, N. Brooks, R. Chase, A. Colleraine, E. Fairbanks, J. Fasolo, R. Fisher, R. Groebner, T. Hino, R. Hong, G. Jahns, J. Kamperschroer, J. Kim, A. Lieber, J. Lohr, D. McColl, L. Rottler, R. Seraydarian, R. Silagi, J. Smith, R. Snider, T. Taylor, J. Tooker, D. Vaslow, and S. Wojtowicz, Nucl. Fusion **24**, 183 (1984).

[4]A. Tanga, K. H. Behringer, A. E. Costley, M. Brusati, B. Denne, A. Edwards, A. Gibson, R. D. Gill, N. Gottardi, R. Granetz, P. J. Harbour, H. Jackel, M. Keilhacker, E. Lazzaro, M. Malacarne, P. D. Morgan, P. Noll, J. Orourke, P. E. Stott, D. R. Summers, J. A. Tagle, and P. R. Thomas, Nucl. Fusion **27**, 1877 (1987).

[5]S. Sengoku, A. Finahashi, M. Hasegawa, K. Hoshino, S. Kasai, T. Kawakami, H. Kawashima, T. Matoba, T. Matsuda, H. Matsumoto, Y. Miura, M. Mori, H. Ogawa, T. Ogawa, H. Ohtsuka, T. Shoji, N. Suzuki, H. Tamai, Y. Uesugi, T. Yamamoto, and T. Yamauchi, Phys. Rev. Lett. **59**, 450 (1987).

[6]K. Toi, K. Kawahata, S. Morita, T. Watari, R. Kumazawa, K. Ida, A. Ando, Y. Oka, M. Sakamoto, Y. Hamada, K. Adati, R. Ando, T. Aoki, S. Hidekuma, S. Hirokura, O. Kaneko, A. Karita, T. Kawamoto, Y. Kawasumi, T. Kurota, K. Masai, K. Narihara, Y. Ogawa, K. Ohkubo, S. Okajima, T. Ozaki, M. Sasao, K. N. Sato, T. Seki, F. Shimpo, H. Takahashi, S. Tanahashi, Y. Taniguchi, and T. Tsuzuki, Phys. Rev. Lett. **64**, 1895 (1990).

[7]C. E. Bush, R. J. Goldston, S. D. Scott, E. D. Fredrickson, K. McGuire, J. Schivell, G. Taylor, C. W. Barnes, M. G. Bell, R. L. Boivin, N. Bretz, R. V. Budny, A. Cavallo, P. C. Efthimion, B. Grek, R. Hawryluk, K. Hill, R. A. Hulse, A. Janos, D. W. Johnson, S. Kilpatrick, D. M. Manos, D. K. Mansfield, D. M. Meade, H. Park, A. T. Ramsey, B. Stratton, E. J. Synakowski, H. H. Towner, R. M. Wieland, M. C. Zarnstorff, and S. Zweben, Phys. Rev. Lett. **65**, 424 (1990).

[8]K. Hoshino, T. Yamamoto, H. Kawashima, N. Suzuki, Y. Uesugi, M. Mori, H. Aikawa, S. Kasai, T. Kawakami, T. Matsuda, Y. Miura, K. Odajima, H. Ogawa, T. Ogawa, H. Ohtsuka, T. Shoji, H. Tamai, T. Yamauchi, T. Kondo, I. Nakazawa, C. R. Neufeld, and H. Maeda, Phys. Rev. Lett. **63**, 770 (1989).

[9]S. Tsuji, K. Ushigusa, Y. Ikeda, T. Imai, T. Itami, M. Nemoto, K. Nagashima, Y. Koida, Y. Kawano, T. Fukuda, T. Kondoh, M. Shimada, H. Nakamura, O. Naito, H. Yoshida, T. Nishitani, H. Kubo, K. Tobita, Y. Kusama, S. Ishida, M. Sato, N. Isei, T. Sugie, N. Miya, R. Yoshino, and K. Uehara, Phys. Rev. Lett. **64**, 1023 (1990).

[10]T. H. Osborne, N. H. Brooks, K. H. Burrell, T. N. Carlstrom, R. J. Groebner, W. Howl, A. G. Kellman, L. L. Lao, T. S. Taylor, D. N. Hill, N. Ohyabu, and M. E. Perry, Nucl. Fusion **30**, 2023 (1990).

[11]B. J. D. Tubbing, B. Balet, D. V. Bartlett, C. D. Challis, S. Corti, R. D. Gill, C. Gormezano, C. W. Gowers, M. von Hellermann, M. Hugon, J. J. Jacquinot, H. Jaeckel, P. Kupschus, K. Lawson, H. Morsi, J. O'Rourke, D. Pasini, F. G. Rimini, G. Sadler, G. L. Schmidt, D. F. H. Start, P. M. Stubberfield, A. Tanga, and F. Tibone, Nucl. Fusion **31**, 839 (1991).

[12]R. J. Taylor, M. L. Brown, B. D. Fried, H. Grote, J. R. Liberati, G. J. Morales, P. Pribyl, D. Darrow, and M. Ono, Phys. Rev. Lett. **63**, 2365 (1989).

[13]R. R. Weynants and R. J. Taylor, Nucl. Fusion **30**, 945 (1990).

[14]R. J. Groebner, K. H. Burrell, and R. P. Seraydarian, Phys. Rev. Lett. **64**, 3015 (1990).

[15]K. H. Burrell, T. N. Carlstrom, E. J. Doyle, P. Gohil, R. J. Groebner, T. Lehecka, N. C. Luhmann, Jr., H. Matsumoto, T. H. Osbone, W. A. Peebles, and R. Philipona, Phys. Fluids B **2**, 1405 (1990).

[16]E. J. Doyle, R. J. Groebner, K. H. Burrell, P. Gohil, T. Lehecka, N. C. Luhmann, Jr., H. Matsumoto, T. H. Osborne, W. A. Peebles, and R. Philipona, Phys. Fluids B **3**, 2300 (1991).

[17]K. Ida, S. Hidekuma, Y. Miura, T. Fujita, M. Mori, K. Hoshino, N. Suzuki, and T. Yamauchi, Phys. Rev. Lett. **65**, 1364 (1990).

[18]S.-I. Itoh and K. Itoh, Phys. Rev. Lett. **60**, 2276 (1988).

[19]S.-I. Itoh and K. Itoh, Nucl. Fusion **29**, 1031 (1989).

[20]S.-I. Itoh and K. Itoh, J. Phys. Soc. Jpn. **59**, 3815 (1990).

[21]K. C. Shaing and E. C. Crume, Jr., Phys. Rev. Lett. **63**, 2369 (1989).

[22]K. C. Shaing, E. C. Crume, Jr., and W. A. Houlberg, Phys. Fluids B **2**, 1492 (1990).

[23]A. B. Hassam, T. M. Antonsen, Jr., J. F. Drake, and C. S. Liu, Phys. Rev. Lett. **66**, 309 (1991).

[24]M. Tendler and V. Rozhansky, Comments Plasma Phys. Controlled Fusion **13**, 191 (1990).

[25]H. Biglari, P. H. Diamond, and P. W. Terry, Phys. Fluids B **2**, 1 (1990).

[26]Y. B. Kim, P. H. Diamond, and R. J. Groebner, Phys. Fluids B **3**, 2050 (1991).

[27]K. Ida and S. Hidekuma, Rev. Sci. Instrum. **60**, 867 (1989).

[28]R. J. Fonck, D. S. Darrow, and K. P. Jaehnig, Phys. Rev. A **29**, 3288 (1984).

[29]K. Hoshino, T. Yamamoto, H. Kawashima, T. Yamauchi, T. Shoji, N. Suzuki, and Y. Uesugi, J. Phys. Soc. Jpn. **58**, 1248 (1989).

[30]Ch. P. Ritz, R. D. Bengtson, S. J. Levinson, and E. J. Powers, Phys. Fluids **27**, 2965 (1984).

[31]K. C. Shaing (private communication).

[32]K. C. Shaing Phys. Fluids B **4**, 290 (1992).